ORIGINAL PAPER

Ferromagnetic, Optical and Photoluminescence Behavior of Ni-Doped ZnO Thin Films

L. Suganya[1] · K S. Balamurugan[2] · A. Sivakami[3] · P. Sakthivel[4] · Nidhi Asthana[5,6] · B. Sundaresan[1]

Abstract

Ni-doped ZnO (NZO) thin films were prepared onto a glass substrate with varying concentrations of 2, 4, 6, 8, 10% of Ni using sol-gel spin coating method and their structural, optical and magnetic characteristics were discussed with supporting of XRD, UV, Photoluminescence, XPS and vibrating sample magnetometer (VSM) characterization techniques. The XRD analysis shows that the polycrystalline hexagonal wurtzite structure with (002) orientation of NZO thin films. The XPS results confirmed the presence of Ni ion in all the samples. The optical bandgap of the prepared samples was decreased with increasing concentrations of nickel from 3.33 to 3.22 eV. Photoluminescence spectra showed a red shift of near band edge (NBE) and deep level (DLE) emissions for prepared undoped and NZO thin films. The VSM of prepared NZO thin films exhibit ferromagnetic behavior at room temperature for potential applications in various fields. Our experimental observations support for transparent conducting electrode and spintronics device applications.

✉ A. Sivakami
  sivakamitce@gmail.com

✉ B. Sundaresan
  suganya02051983@gmail.com

[1] Department of Physics, Centre For Research and Post Graduate Studies, Ayya Nadar Janaki Ammal College (Autonomous), Sivakasi, Tamil Nadu 626123, India

[2] Department of Electronics and Communication Engineering, Karpaga Vinayaga College of Engineering and Technology, Chengalpattu, Tamil Nadu 603308, India

[3] Department of Physics, Sri Eshwar College of Engineering, Kinathukadavu, Coimbatore, Tamil Nadu 641202, India

[4] Department of Physics, Science and Humanities, Centre for Materials Science, Faculty of Engineering, Karpagam Academy of Higher Education, Coimbatore, Tamil Nadu 641105, India

[5] Department of Physics, Babasaheb Bhimrao Ambedkar University, Lucknow, Uttar Pradesh, India

[6] Department of Physics, Graphic Era (Deemed to be University), Dehradun, Uttarakhand, India

Graphical Abstract
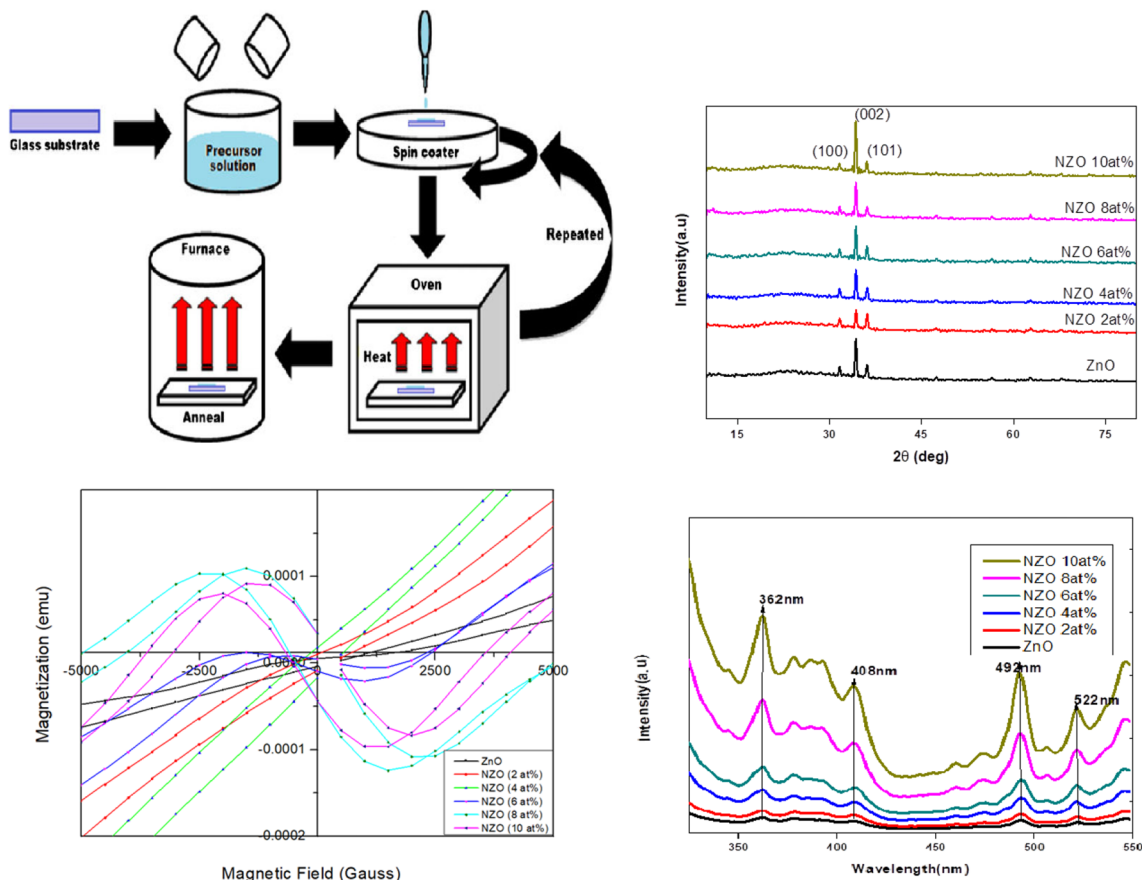
1 Introduction

TCO films are widely used in thin film technology owing to their significant applications in different fields. ZnO films are one of the TCO films and attracted the researchers to fabricate spintronic devices due to their wide bandgap (3.3 eV), low dielectric constant, large excitation binding energy, thermal conductivity, high electron mobility and high optical transmittance, strong luminescence under low temperature, non-toxic and abundant in nature [1–3]. ZnO is effectively used as the active layer, substrate and anti-reflection coating material in solar cells. ZnO's growing interest arises because of its potential applications in sensors, solar cells, piezoelectric devices, light-emitting diodes, photocatalytic,

drug-delivery and antibacterial activities [4–8]. ZnO materials are important potential candidate from optoelectronics to bio medicine.The transition element Ni has a good conductor of heat and electricity and loses its metallic characteristics very slowly than other transition elements. Nickel-doped ZnO thin films are excellent materials for different properties like good optoelectronic, electrical, luminescence and thermal properties without changing the crystalline structure of zinc oxide. To achieve the photo electrical and solar cell applications based on ZnO thin films relatively dependent on the low energy band gap. This low-energy band gap is controlled by different dopant and synthesis methods.

Both band gap and optical absorption shift of ZnO films are tuned by doping different transition metals

like Ni, Cu, Mn, Fe, etc. [9–11]. Liton et al. concluded that other elements like Cu and N doping with ZnO may change the crystalline plane structure [12]. In addition to that dilute magnetic semiconductors (DMS) are found to have wide-field applications in spin electronics. Metal ions are used to substitute group II or group IV elements in II–VI or IV–VI semiconductor compound alloys.

The large spin-dependent properties of DMS are having the excellent potential of achieving the external control of spin in the presence of a magnetic field which is useful in spintronics applications. Also, the structural, morphological, optoelectronic and magnetic properties of DMS thin films are varied by doping the different elements like Al, Fe, Co, Mn, Mg and Pb for various applications in different fields [13].

There are several methods for creating thin films, including thermal evaporation, chemical vapor deposition (CVD), molecular beam epitaxy (MBE), pulse laser deposition, sputtering, dip coating, spray pyrolysis and spin coating. Among all these techniques, the spin coating technique is good for even coating doped ZnO films at a low cost. The nickel doping effect on ZnO thin films is significantly important in applications based on the type of growth technique used. ZnO structural and optical properties were modified in terms of substrate temperature, disk rotation and pressure of the chamber during growth. Several researchers are investigated to achieve the low energy band gap by selecting of different synthesis methods as well as parameters are also optimized for various applications. Several research papers are reported that the ZnO energy band gap is reduced when nickel doping content is increased beyond 3% and also it is a relatively dependent synthesis method.

In the present paper, nickel-doped ZnO thin films have been prepared with 2-Methoxy ethanol as a solvent which has not been tried by earlier investigators. The films are prepared and characterized for optical, structural and magnetic properties.

2 Experimental Details

2.1 Substrate Cleaning

Microscope glass substrates were used for the deposition of Ni-doped ZnO film deposition. The substrates were first cleaned with the soap solution and then soaked in concentrated HCl acid for 1 day. The soaked substrate was cleaned again using distilled water in an ultrasonic cleaning bath for 30 min and then rinsed with acetone. After these processes, the substrates were dried with a hot plate at $100\,^{\circ}$C for 5 min and cooled to room temperature.

2.2 Material Used

Zinc acetate dihydrate is used as a precursor, Nickel acetate tetrahydrate as a dopant and 2 Methoxy ethanol and Monoethanolamine are used as solvent and stabilizers. AR/BDH grade chemicals were purchased and used.

2.3 Solution Preparation

The precursor solution was prepared by dissolving 2.197 gm of Zinc acetate dihydrate in 20 ml of 2-Methoxy ethanol for 0.5 M concentration and stirred at $70\,^{\circ}$C for 1 h which forms an acidic solution. Then monoethanolamine was added dropwise and the solution was stirred at $70\,^{\circ}$C for 1 h which gives the clear homogeneous solution. It was aged for 1 day and used to deposit ZnO films.

Nickel was doped for various concentrations (2, 4, 6, 8, 10 at%) to get NZO thin films. Zinc acetate dihydrate and Nickel acetate tetrahydrate were dissolved in 2-Methoxy ethanol for 1 h at $70\,^{\circ}$C. An appropriate amount of MEA was added drop by drop and the solution was stirred at $70\,^{\circ}$C for 1 h. The solution was aged at room temperature for 1 day and used to deposit NZO films.

2.4 Film Formation

Using a spin coater, the prepared sol was deposited onto a clean piece of glass and spun for 30 S at 3000 rpm. After each coating, the film was preheated at $150\,^{\circ}$C for 10 min and then cooled for 10 min to evaporate and remove organic residuals. This process was repeated to coat 8 layers to get desired film thickness. Finally, the films were post-annealed in muffle furnace at $450\,^{\circ}$C for 2 h to get crystallized ZnO films.

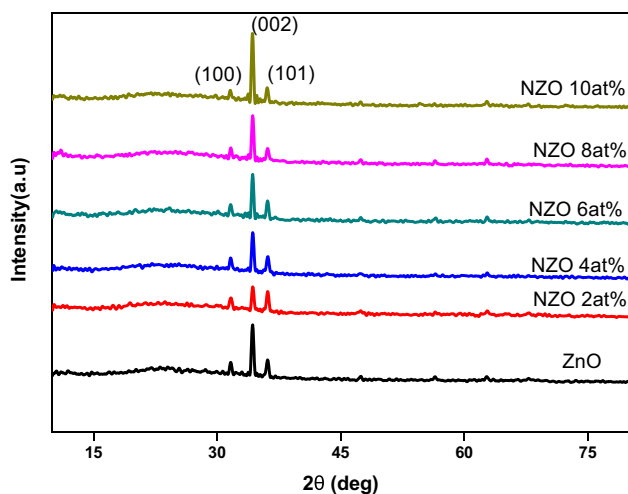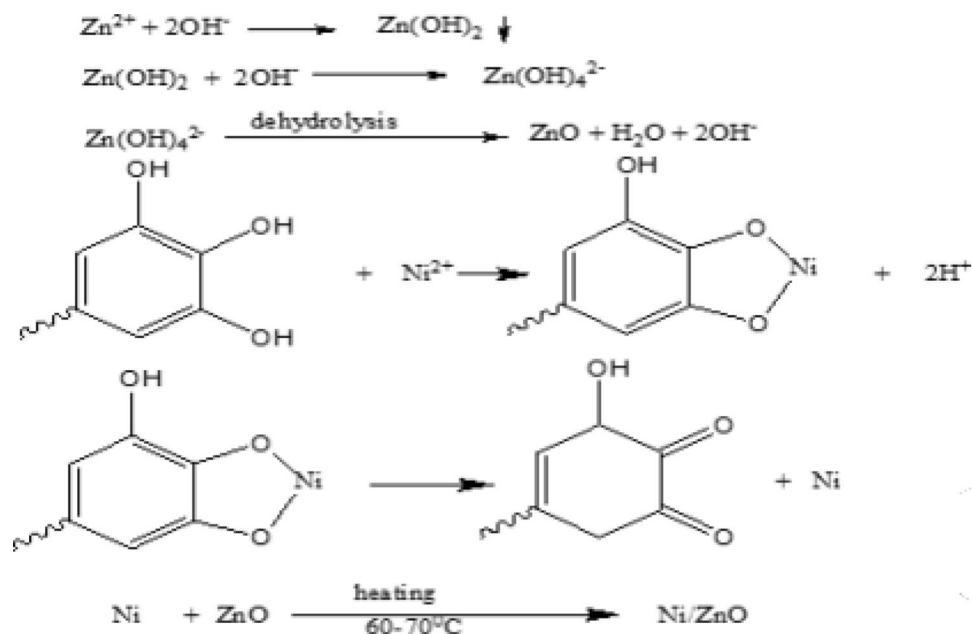Chemical reaction mechanism of Ni-doped ZnO films

Fig. 1 XRD pattern for undoped and NZO thin films

3 Results and Discussion

3.1 Structural Properties XRD Parameters

It was observed from the Fig. 1. that the undoped ZnO film exhibited the Bragg's diffraction peaks at the diffraction angle 2q are 31° 61′, 34° 30′ and 36° 17′ corresponding to (100), (002) and (101) planes. The preferential orientation of ZnO film is found to be along the (002) Plane. The results were compared with JCPDS card no: 36-1451 [14]. The intensity of the (002) plane is found to be higher than that of (100) and (101) planes. On doping Ni at 2 at% concentration, no peak shifting was observed and the preferential orientation (002) of ZnO film has also not been changed. But, the intensity of the peak seems to be reduced. When the Ni doping concentration is increased to 4 at%, the same results were obtained but in contrast, the intensity of the peak has been increased. Similarly, the NZO films with Ni doping concentrations 6, 8 and 10 at% also showed an increase in intensity without any change in peak position and preferential orientation. The observed change in intensity ascertained the incorporation of Ni ion into the ZnO lattice. The difference in intensity is also ascribed to the film thickness. The obtained Bragg's peaks indicated that both undoped and Ni-doped ZnO films have been crystallized under the hexagonal wurtzite structure. NiO, Zn or Ni secondary phases have not been found. Due to the Piezoelectric effect, which facilitates the simpler separation of carrier charges, the preferential orientation along (002) direction supported the benefit for transport properties [15].

Experimental values of X-ray, diffraction angle and full width half maximum value of peaks are used to calculate microstrain, crystalline size, lattice constants, stress, dislocation density, number of crystallites and texture coefficients. The calculated values are tabulated and compared.

Table 1 Plane of orientation, crystallite size, texture coefficient and lattice constant for the prepared samples

Sample	2 degree	(hkl) plane	Crystallite size nm		Texture coefficient along (002) plane	Lattice constant
			Debye Scherrer method	W-H plot		
UndopedZnO	34.3049	(002)	33.81	35.2	2.62649	1.732051
ZnO:Ni(2 at%)	34.3159	(002)	37.64	38.1	2.205389	1.732051
ZnO:Ni(4 at%)	34.3195	(002)	41.63	39.4	2.588677	1.732051
ZnO:Ni(6 at%)	34.3187	(002)	43.37	41.3	2.613606	1.732051
ZnO:Ni(8 at%)	34.2995	(002)	46.18	45.2	2.766575	1.732051
ZnO:Ni(10 at%)	34.1319	(002)	37.47	39.6	2.708056	1.732051

Microstrain in the deposited thin films is defined as the root mean square of the variation in the lattice parameters across the sample. It is computed and scrutinized for a better understanding of the crystallography structure of NZO films [16]. The strain is very minute and it is the measure of deformation from the ideal lattice. The crystal defects and distortion arising during the growth of crystalline structure in the films have led to a strain in the films [17] and it is evaluated by the relation [18].

$$\varepsilon = \frac{\beta \cos\theta}{4} \tag{1}$$

The scrutiny of strain values revealed that the strain significantly decreased for NZO films when compared with undoped ZnO films. This may be due to the improvement in the crystalline nature because of the reduction in the number of crystal defects arising out of Ni doping. 8 at% Ni-doped ZnO film showed a higher reduction in microstrain value which may be attributed to the larger level of reduction in the number of crystal defects at the particular concentration. The crystal quality of the ZnO films is decided by the crystallites size (D), calculated using the following Debye-Scherrer Eqs. [19],

$$D = \frac{\lambda k}{\beta \cos\theta} \tag{2}$$

where, $k = 0.9$ is the Scherrer constant, $\lambda = 0.15418$ nm is the radiation wavelength, β is the FWHM and θ is the peak position at 34° corresponding to (002) plane.

The crystallite size of undoped ZnO is determined as 33.81 nm. On doping of 2 at% Ni, it increases to 37.64 nm. Further increase of Ni doping concentration to 4, 6, 8 and 10at% resulted in the size 41.63, 43.37, 46.18 and 37.47 nm. Agglomeration may be the cause of the increased crystallite size observed with rising Ni concentrations. This is further confirmed by the decrease in the value of lattice parameters from 5.2239 to 5.2222, 5.2217, 5.2218 Å, for 2, 4, 6 and 10 at% of Ni doping. But for 8 at% it increases to 5.2247 Å which revealed the occurrence

of a higher agglomeration at this particular concentration [20]. The constant value of the c/a ratio of undoped and Ni-doped ZnO films revealed that the hexagonal wurtzite structure of ZnO has not been changed by the addition of Ni. The variation of stress also substantiated the above conclusion that the agglomeration is higher at 8 at% Ni doping. The increase in D size confirmed the improvement in the stoichiometry of films due to the lowered dislocation density and hence the microstrain [21]. The crystallite size of the prepared combination of materials was verified through W-H plot showed in Fig. 2 and it is also included in the Table 1.

In contrast, at 10 at% the crystallite size significantly decreases to 37.47 nm which confirmed the nickel incorporation into the ZnO lattice. A similar observation has been made by sindhu et al., for cobalt doping in ZnO films.

3.2 XPS and EDS Analysis

The chemical composition and chemical state of ZnO and Ni (0%, 25% and 4%) doped ZnO thin films are analyzed using XPS in Fig. 3. There are no impurity peaks and the indexed peaks may be ascribed to Zn, Ni, O and C elements. The Ni-related peaks were attained at eV 853.21. The existence of the Ni peaks demonstrated that the doping procedure was successful. Two peaks, 2p3/2 and 2p1/2, were visible in the Zn 2p spectra at energies of 1021.39 eV and 1044.45 eV, respectively. The presence of this peak is determined by the spin-orbit coupling. The interaction of Ni with ZnO causes the positions of these peaks to shift toward higher energy values. The XPS instrument's vacuum system uses pump oil, and as a result, the carbon component is present. Here, the binding energy calibration reference point is the carbon C 1s peak at 284.8 eV. Figure 4. displays the EDS spectra of Ni-doped and undoped ZnO thin films. Each EDS shot has an inset displaying the atomic percentages of Zn, O and Ni. The obtained data supported the target stoichiometry ratio's dopant composition. The prepared samples had no
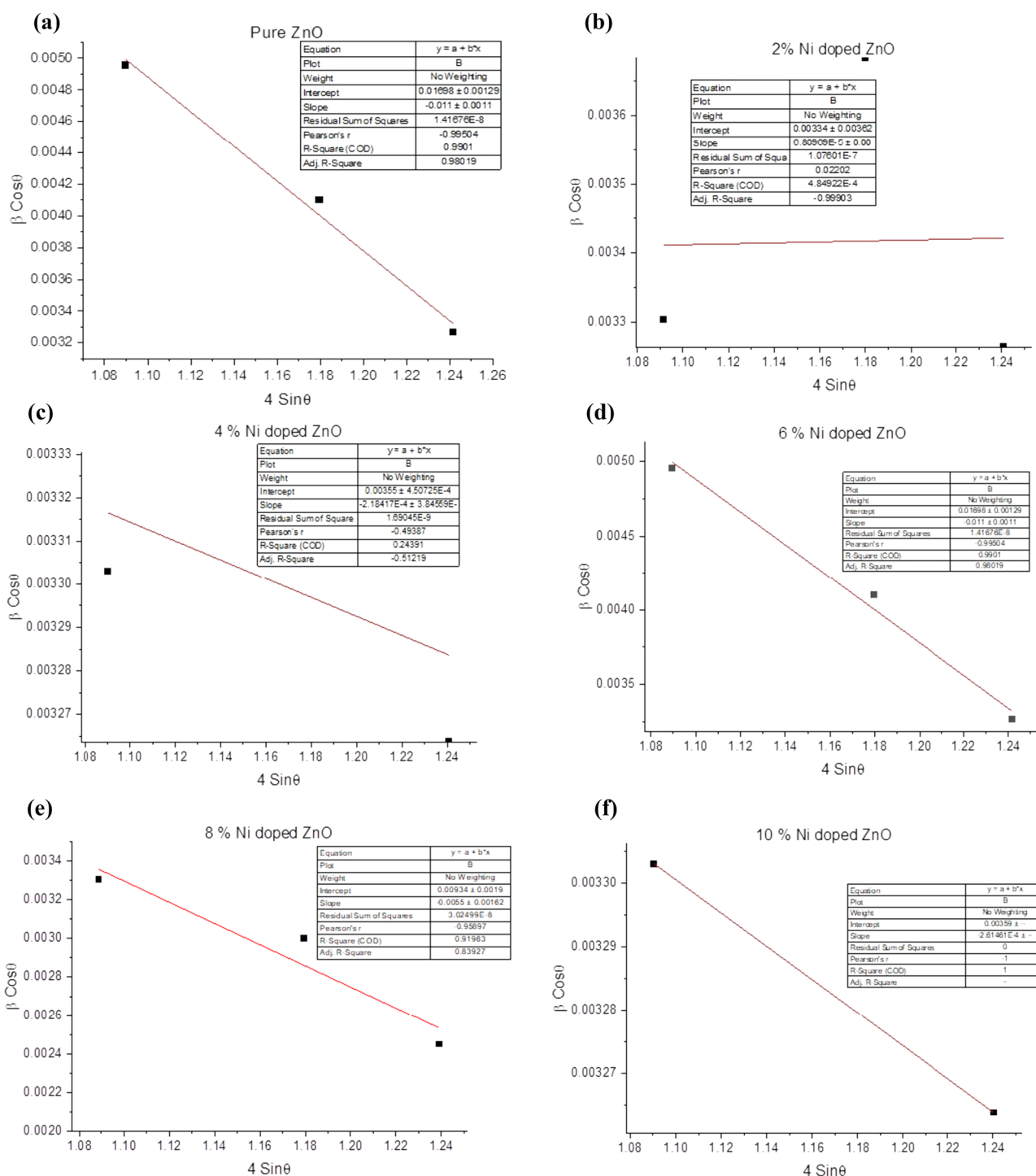
Fig. 2 **a–f** W-H plots of undoped and NZO thin films. **a** Pure ZnO thin film. **b** 2% Ni doped ZnO thin film. **c** 4% Ni doped ZnO thin film. **d** 6% Ni doped ZnO thin film. **e** 8% Ni doped ZnO thin film. **f** 10% Ni doped ZnO thin film

contaminants, and the EDS spectra proved that the doping was efficient.

3.3 UV-Vis Transmittance Studies

Figure 5 shows the transmittance spectra of the ZnO:Ni films as determined by UV-VIS spectroscopy in the 200–1000 nm

Fig. 3 XPS analysis of undoped and NZO thin films
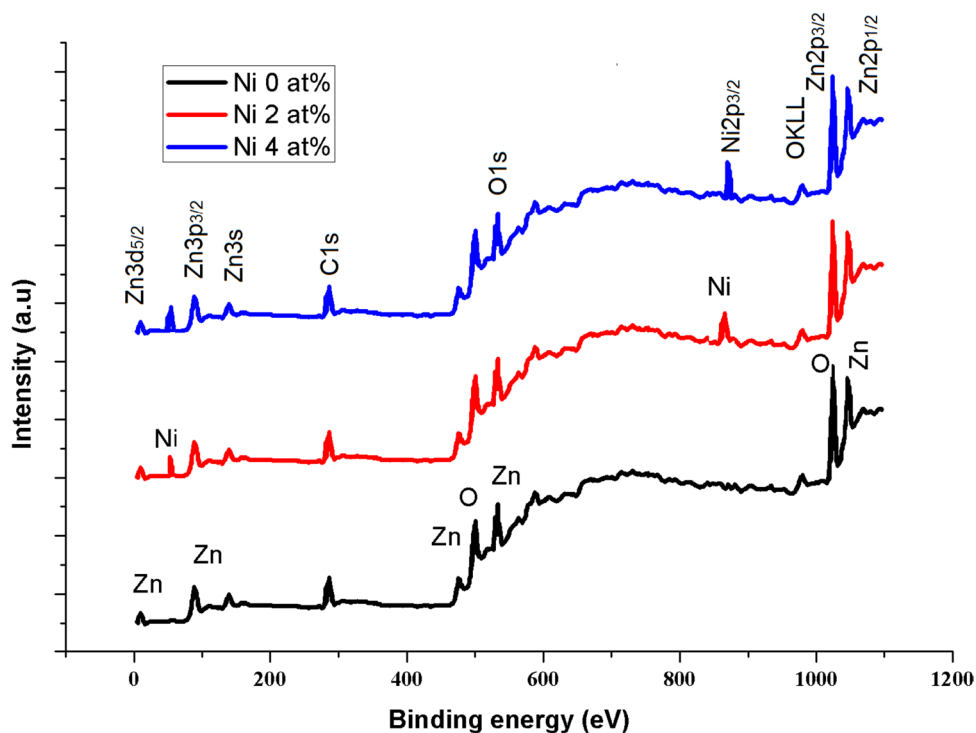
region. The transmittance of undoped ZnO film was determined as 91% where as it is reduced to 82% and 81% for 2 and 4 at %. At 6 at % and 8 at% it was about 68 nm and 67 nm respectively. Transmittance was sharply decreased at about 370 nm for both the doped and undoped films which is attributed to the band edge absorption. This is understood as the incoming photons having sufficient energy to excite electrons from the valence band to the conduction. As the Ni doping concentration increases the transmittance was reduced and higher reduction was observed at 6 at% and 8 at% of Ni doping. The reduction in transmittance may be due to the increased thickness of the doped films and due to the increased lattice distortion or defects [22]. Variation in the sharp drop of transmittance was observed for both doped and undoped films which revealed that Ni-related defect states are present in the forbidden band which leads to enhanced absorption [23].

The host XIIYVI(ZnII OVI) semiconductor's (II-VI group) band structure may change as a result of the doping of Ni, which also produces novel optical transitions. When Zn (X) host atom is replaced by Ni, the band gap is altered and hence the optical absorption is varied. It is confirmed by the observed absorption in the visible part of the spectrum. Especially around 600 nm. This can be explained by the existence of d–d′ transition bands around 600 nm which are the characteristics of Ni (II) with tetrahedral symmetry [24]. Therefore, the nickel incorporation has also led to the multiple Ni^{2+} internal transitions present in Zno:Ni films

which are reflected in the variation in the sharpness of higher energy absorption edge for the Ni-doped films. This in turn becomes evidence for the substitution of the dopant ions in Zno.

The optical bandgap energy (E_g) was calculated from transmission spectra. The variation of ($\alpha h\nu)^2$ with photon energy ($h\nu$) was found to give the relation as

$$(\alpha h v)^2 = A\left(hv - E_g\right)^{1/2} \tag{3}$$

where A is constant, α is an absorption coefficient and Eg is the optical bandgap energy [25]. For Ni-doped ZnO thin films made with various Ni concentrations, the fluctuation of ($\alpha h\nu)^2$ versus h.

These Taucs plots are shown in Fig. 6. The optical bandgap values estimated from the Taucs plots are given in Table 2.

It can be seen from Table 2 that the optical band gap values of Ni-doped films are decreasing against the increasing concentration of Ni. Moreover, the Eg values of Ni-doped films are lesser than that of the undoped ZnO films. This is ascribed to the s-d and p-d interactions causing band gap kneeling, which second-order perturbation theory could explain [26]. Further, it can be stated that the bandgap kneeling is due to the activation of "spd" exchange interactions [27]. Also, the entrance of the Ni state at the top of the valence band may be responsible for the bandgap narrowing with increasing Ni content [10, 28].
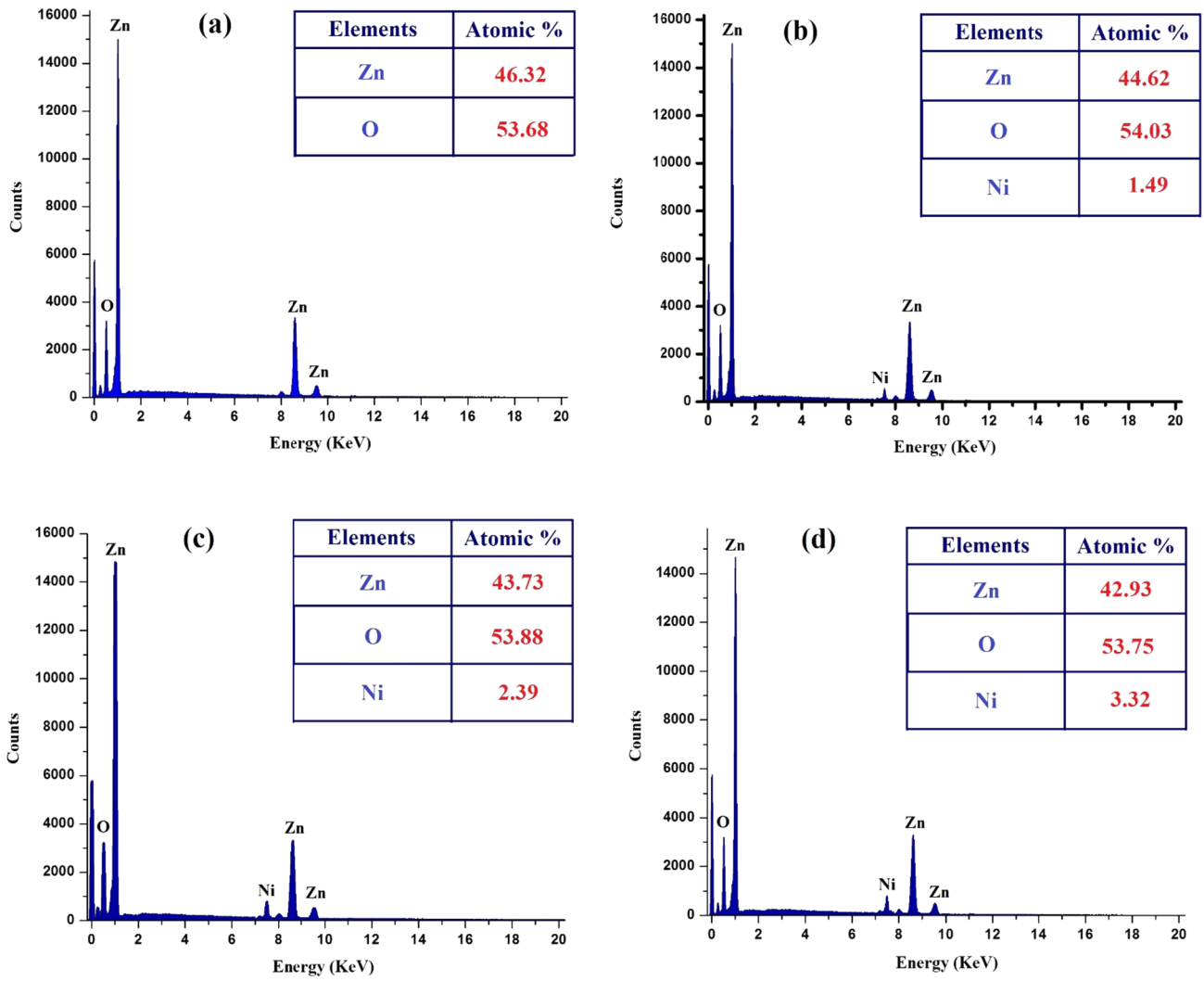
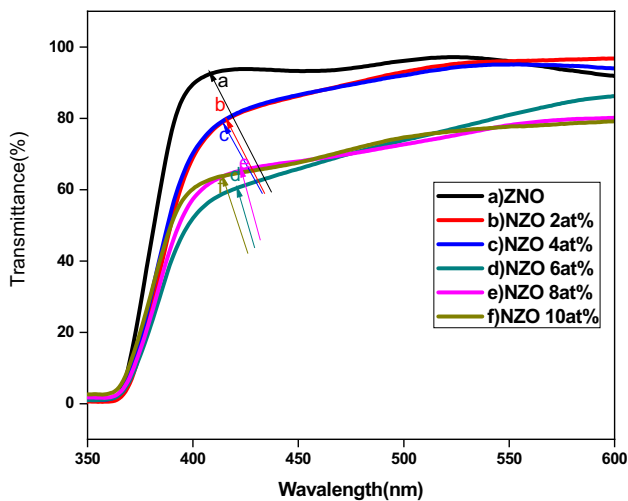**Fig. 4** EDS results of undoped and NZO thin films

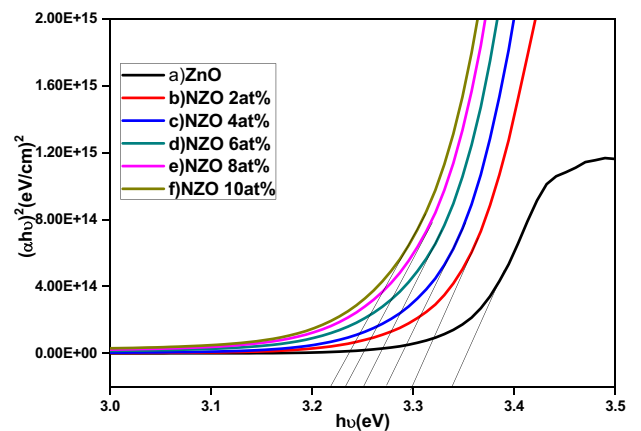**Fig. 5** Transmittance spectra for undoped and NZO thin films

Fig. 6 Tauc's plot for undoped and NZO thin films

Table 2 Micro strain, stress, dislocation density, number of crystallite per unit area for the prepared samples

| Sample	Micro strain (με)	Stress θ (Pa)	Dislocation density × 10^{14} lines/m^3	Thickness (nm)	Number of crystallite per unit area
Undoped ZnO	0.001025	− 0.77321	8.75	1860	4.8181×1016
ZnO:Ni(2 at%)	0.000921	− 0.70031	7.06	4520	8.4757×1016
ZnO:Ni(4 at%)	0.000833	− 0.67654	5.77	1610	2.2308×1016
ZnO:Ni(6 at%)	0.000799	− 0.68209	5.32	1450	1.7773×1016
ZnO:Ni(8 at%)	0.000751	− 0.80888	4.69	2350	2.3852×1016
ZnO:Ni(10 at%)	0.000925	− 0.67971	7.12	2300	4.3715×1016
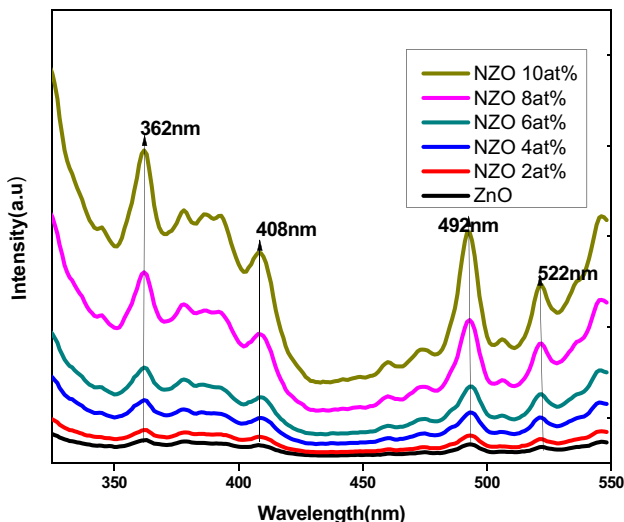
Fig. 7 PL spectra for undoped and NZO thin films

Table 3 Transmittance and energy band gap values for the prepared samples

Sample	Transmittance (%)	Wavelength (nm)	Energy band gap (eV)
Undoped ZnO	91	403	3.3396
ZnO:Ni(2 at%)	82	430	3.3001
ZnO:Ni(4 at%)	81	418	3.2736
ZnO:Ni(6 at%)	68	452	3.2528
ZnO:Ni(8 at%)	67	436	3.2348
ZnO:Ni(10 at%)	62	412	3.2208

3.4 Photoluminescence Studies

Photoluminescence spectroscopic study is usually carried for ZnO thin films to identify the presence of different intrinsic defects in doped ZnO films by determining various radiative recombination and trapping levels of the photo-generated electrons and holes [29, 30]. In the present study, a systematic investigation of the influences of Ni doping on the PL spectra of all NZO films was performed and the spectra as shown in Fig. 7.

As seen in Fig. 7, both the doped and undoped ZnO films show emission peaks at 362, 408, 492 and 522 nm. Thus, the emission peaks are in both the UV region and in visible luminescence (VL) region. The UV emission peak at 362 nm originated from the ZnO near band edge (NBE) transition and is normally ascribed to this free exciton's recombination [31]. Table 3 gives the value of transmittance and energy band gap of the prepared samples with different concentrations.

The VL peaks are 408, 492 and 522 nm and are attributed to deep-level emissions by different types of intrinsic defect states, such as Zni, Oi, VZn, Vo and Ozn in the ZnO lattice [32]. In ZnO, the defect energy states of Oi and Vzn are generated closer to the valence band (VB) whereas the level of Zni and Vo are generated closer to the conduction band (CB) [31]. The possible electronic transitions in ZnO films are as follows.

1. The transition between Zni(extended Zni) levels and the VB.
2. The transition between the bottom of the CB and the Zni level and.
3. The transition between the VB and the Oi/Volevels.

Emission due to the above transition is not well resolved in the spectrum of pure ZnO but it could be resolved in the Ni-doped films. The intensity of both UV and VL peaks is significantly enhanced and becomes broadened with defined shapes. This may be due to the generation of different intrinsic defects by Ni doping. Similar observations have been made by many researchers [33, 34]. Enhancement of the intensity of the UV band may be ascribed to the generation of the increased number of photo excitons and their recombination rate. The asymmetric nature of PL spectra implied the superposition of multiple emission bands. The spectra showed one UV peak around 362 nm and three emission peaks in the visible region around 408, 492 and 522 nm. It is
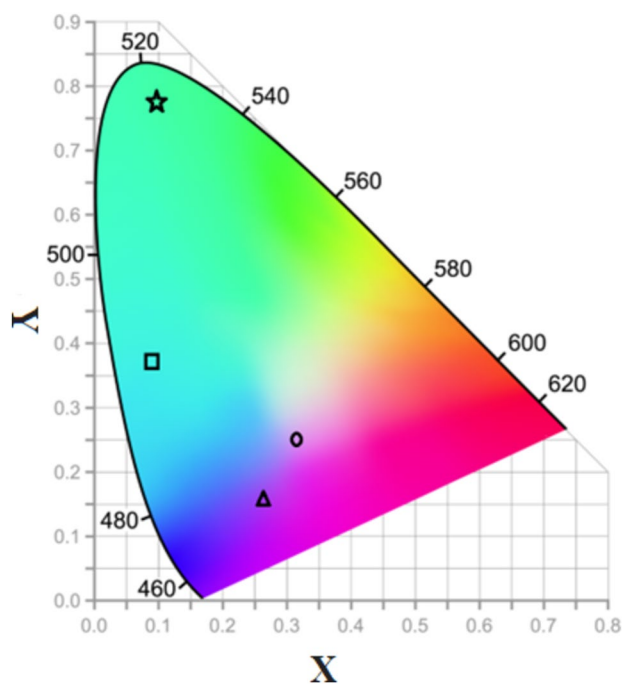
Fig. 8 CIE chromaticity diagram of NZO thin films

also observed that both UV and VL bands showed a red shift against the increase of Ni doping which confirmed the substitution of Ni ions in the Zn sites in the lattice. The redshift of UV peaks revealed a strong sp-d exchange interaction. Generally, it is stated that the VL emissions arise out of the different structural point defects in the lattice, but still it is under debate. The exact identification of VL emission due to the specific point defects is still in controversial [35]. Most commonly, blue-violet emissions are observed in ZnO which is generally attributed to the Zn-related defects. Likewise, the green emission bands are believed to originate from both Vo and VZn defects [36]. Recombination of trapped holes at VZn with trapped electrons at the Zn is hallow level [37] or trapped electrons recombining with photogenerated holes at high levels of Zni [38] or the combined effect of these two may be responsible for violet-blue emission. Thus, the blue emission at 492 nm corresponds to a transition between the VZn level and the bottom of the CB level. Similar results were observed by the earlier investigators. The peak centered at 408 nm is ascribed to the Oi.

The emission band observed at 522 nm can be attributed to both Vo and VZn states since these states are indistinguishable due to the slight difference in their peak positions. According to the earlier reports, the green emission at 522 nm was ascribed to the presence of the defect Voand hence the transition from Vo acceptor level to the VB [39–47]. As a whole, both undoped and Ni-doped ZnO films showed similar features of PL spectra with emission peaks centered almost at the

same wavelength. However, significant enhancement in the intensity of bands UV and VL region was observed against the increase of Ni doping concentration. This is strong evidence for the enhancement of intrinsic defects in ZnO films induced by Ni doping. The corresponding CIE chromaticity diagram is given in Fig. 8. In this case of green emission, the enhancement of intensity proved that the Vo concentration increased against the increase of Ni doping concentration.

3.5 Magnetic Properties

The Vibrating Sample Magnetometer (VSM) was used to test the magnetic hysteresis of thin ZnO: Ni films at ambient temperature. Representative RT magnetization curves of $Zn_{1-x}Ni_xO$ films with different Ni concentration are shown in Fig. 9. Undoped ZnO film showed a ferromagnetic behavior which is in accordance with earlier investigations. Also Ni doped films showed ferromagnetic behavior with saturated magnetization. This is also in agreement with earlier results [48]. Ni cluster and NiO in the films do not contribute to the observed ferromagnetism in the NZO films because no evidence for the secondary phase NiO or Ni cluster was observed in XRD measurements. Therefore, it may be said that the observed ferromagnetism is a characteristic of NZO films themselves. As the spin-spin coupling in ferromagnetic materials is a long range interaction, the ferromagnetic characteristics of NZO films are mostly related to Ni incorporation and the microstructure of NZO films [49]. Ni incorporation in ZnO films is also evidenced in XRD studies.

The coercive fields are larger for undoped ZnO and for Ni doped films at higher Ni doping concentrations 6, 8 and 10 at%. Similar results have been obtained by earlier investigators [50]. Coercive field of undoped ZnO is 6334.8 Oe whereas it is 174.46 and 355.30 Oes for 2 and 4 at% Ni doping respectively. At higher Ni doping level 6, 8 and 10 at%, the coercive fields are 1921.7, 4842, 2737.5 Oes respectively.

The saturation magnetization values are also higher for NZO films when compared with undoped ZnO films. Retentivity values of NZO films are also higher than undoped ZnO films. Coercivity, Retentivity and Magnetization values are not following any regular trend as increasing and decreasing against the increase of Ni doping concentration and values are listed in the Table 4. But the magnetic ordering induced in the prepared Ni doped ZnO films is originated from several intrinsic sources, as the XRD results ruled out the possibility for any extrinsic phases related to metallic Ni. The ferromagnetic contribution in Ni doped ZnO films is most likely due to different coupling between the localized Ni-Ni moments and between the localized Ni moments and the delocalized charge carriers, say, conduction and valance band
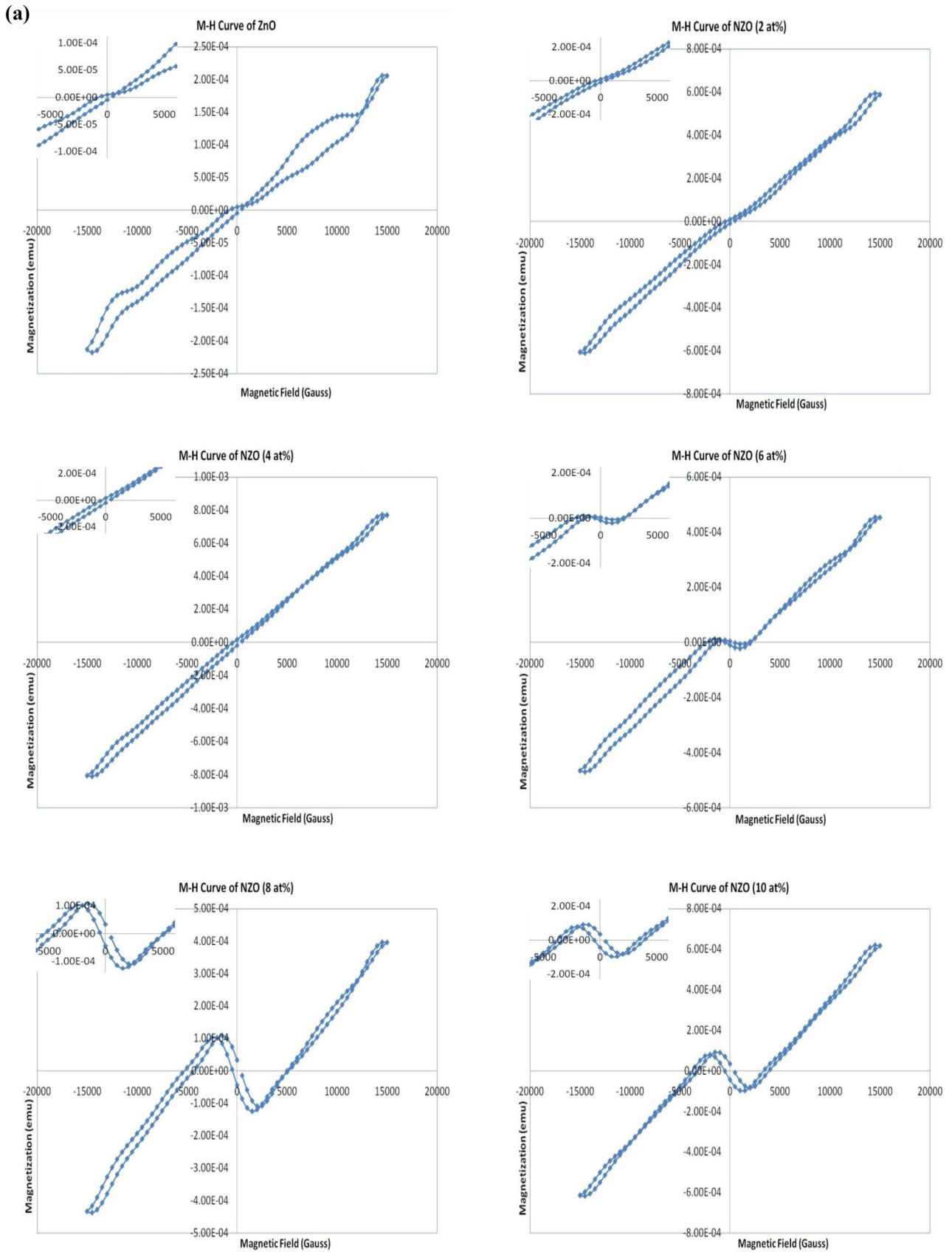
(a)

Fig. 9 **a** M-H curve of undoped and 2, 4, 6, 8, 10% Ni doped thin films, **b** M-H curve for undoped and NZO thin films
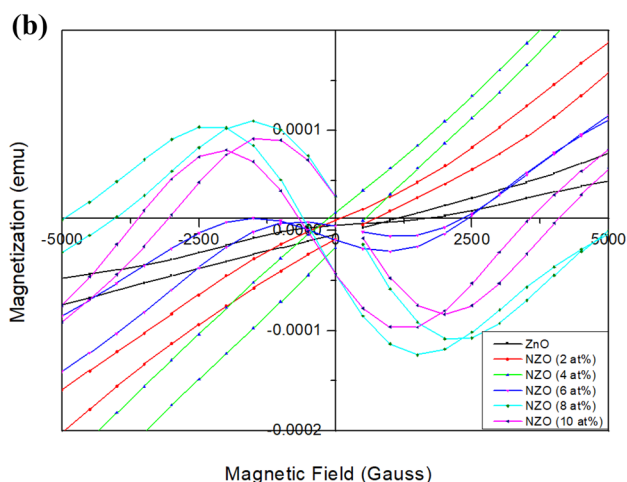
(b)

Fig. 9 (continued)

unoccupied (2+) and doubly occupied (0) states have spin-zero ground states and hence not inducing FM but the singly occupied (1+) state has magnetic moment and hence most likely to contribute to the formation of BMPs. The redshift of optical band gap observed in UV-Vis spectral study also supported the enhancement in Sp-d exchange interaction and the defect, V_o, level. This in turn supported the contribution of Sp-d exchange interaction and V_o levels to the ferromagnetic ordering.

4 Conclusions, Outlook and Future Aspects

Ni doped ZnO thin films have been prepared with Ni concentration varying from 0 to 10 at% in steps of 2 at% by sol-gel spin coating technique and observed the structural,

Table 4 Coercivity, retentivity and magnetization values for the prepared samples

Sample	Coercivity (Oe)	Retentivity (emu)	Magnetization (emu)
Glass	567.69	11.745E-6	200.57E-6
Undoped ZnO	6334.8	4.422E-6	128.44E-6
ZnO:Ni(2 at%)	174.46	3.6135E-6	524.95E-6
ZnO:Ni(4 at%)	355.30	7.1256E-6	712.45E-6
ZnO:Ni(6 at%)	1921.7	27.888E-6	379.98E-6
ZnO:Ni(8 at%)	4842.0	69.929E-6	336.07E-6
ZnO:Ni(10 at%)	2737.5	76.623E-6	537.85E-6

electrons and holes. The delocalized of charge carriers are correlated with different intrinsic defects in the ZnO lattice. Generally, the long-range magnetic ordering in TM doped ZnO is attributed to the possible Sp-d exchange interaction. At the same time, the hole mediated exchange interaction can also produce ferromagnetism (FM) [51]. Normally, the bound magnetic polarons (BMPs) are created in the systems in which Sp-d exchange interaction takes place. This Sp-d exchange interaction may lead to the ferromagnetic ordering of Ni moments at and above RT. Intrinsic defects in the ZnO lattice acts as trapping centre and the electrons are trapped locally by the defect V_o .when the trapped electrons filling the orbitals, it leads to the overlapping with the Ni d-shell.

Enhancement of the defect V_o, concentration has been observed for the increasing Ni concentration in ZnO films by PL spectra. The significant enhancement in the emission band at 522 nm is ascribed to the V_o acceptor level which is confirmed by PL spectra. Increase of saturation magnetization against the increase of Ni doping level clearly indicated that the origin of the magnetic order and it can be correlated to the concentration of V_o level. There are three different charge states for V_o in ZnO lattice as 0, 1+ and 2+. The

optical, luminescent and magnetic properties of NZO thin films. XRD results showed polycrystalline hexagonal wurtzite structure and confirmed the incorporation of Ni onto ZnO lattice. Ni Incorporation enhanced the crystalline quality. The D size also increased after doping except 10 at%. The optical bandgap of Ni doped films showed red shift when compared to pure ZnO film, which may be attributed to the introduction of Ni state in the top of the valence band. PL studies showed NBE and DLE emissions. These emissions are normally ascribed to transition between conduction band and defect levels and free exciton recombination. Magnetic studies showed the ferromagnetic behaviour of NZO films. In addition, the correlation between optical, Pl and Magnetic behaviour has been achieved. The red shift in band gap and emission peak intensities are well correlated with magnetic behavior due to Sp-d exchange interaction and oxygen vacancy levels. The band gap is decreased from 3.33 to 3.22 eV was observed with different Ni doping concentration. The highest magnetization was observed for 4 at% of Ni doped ZnO thin film is found to be 712.45×10^{-6} emu/g. So, the NZO thin films are effective materials for future spintronics and photocatalytic applications.

Declarations

References

1. Ariyakkani P, Suganya L, Sundaresan B (2017) J Alloy Comp 695:3467–3475. https://doi.org/10.1016/j.jallcom.2016.12.011
2. Suganya L, Sundaresan B, Sankareswari G, Ravichandran K, Sakthivel B (2014) J Matter Sci Mater Electron 25:361–368. https://doi.org/10.1007/s10854-013-1595-2
3. Nilavazhagan AD, Santhanam S, Chidhambaram A, Kunavathy N, Tansir Ahamed KV, Alsheri SM (2021) Phys E 129:114665. https://doi.org/10.1016/j.physe.2021.114665
4. Kanagamani K, Muthukrishnan P, Kathiresan A, Shankar K, Sakthivel P, Ilayaraja M (2021) Acta Metall Sin (Engl Lett) 34:729–740. https://doi.org/10.1007/s40195-020-01116-x
5. Shanmugapriya V, Arunpandiyan S, Hariharan G, Bharathi S, Selvakumar B, Arivarasan A (2023) J Alloys Compd 935:167994. https://doi.org/10.1016/j.jallcom.2022.167994
6. Stolyarchuk I, Kuzyk O, Dankliv O, Andrzej D, Kleto G, Andriy S, Adriy P, Hadzaman I (2023) Coatings 13(3):601. https://doi.org/10.3390/coatings13030601
7. Govindaraj M, Babu S, Rathinam R, Vasini V, Vijayakumar K (2023) Chem Pap 77:169–183. https://doi.org/10.1007/s11696-022-02473-w
8. Bagyalakshmi S, Sivakami A, Balamurugan KS (2020) Obes Med 18:100229. https://doi.org/10.1016/j.obmed.2020.100229
9. Aboud AA, Shaban M, Revaprasadu N (2019) RSC Adv 9:7729–7736. https://doi.org/10.1039/C8RA10599E
10. Ali H, Alsmadi AM, Salameh B, Mathai M, Shatnawi M, Hadia NMA, Ibrahim EMM (2020) J Alloys Compd 816:152538. https://doi.org/10.1016/j.jallcom.2019.152538
11. Zhanhong MA, Ren F, Deng Y, Volinsky AA (2020) Optik 219:165204. https://doi.org/10.1016/j.ijleo.2020.165204
12. Ayad AM, Benharrat A, Anas L (2021) Semiconductors 55:482–490. https://doi.org/10.1134/S1063782621050043
13. Saravanakumar K, Sakthivel P, Sankaranarayanan RK (2022). Spectrochim Acta. https://doi.org/10.1016/j.saa.2021.120487
14. Siddheswaran R, Netrvalova M, Savkova J, Novak P, Ocenasek J, Sutta P, Kovac J, Jyavel R (2015) J Alloys Comp 636:85–92. https://doi.org/10.1016/j.jallcom.2015.02.142
15. Jilani A, Abdel-wahab M, Sh., Al-ghamdi AA, Dahlan A, Yahia IS (2016) Phys B Condens Matter 481:97–103. https://doi.org/10.1016/j.physb.2015.10.038
16. Kayani ZN, Riaz S, Naseem S (2019) Mater Res Exp 6:036404. https://doi.org/10.1088/2053-1591/aaf3c8
17. Sakthivel P, Muthukumaran S (2016) J Inorg Organomet Polym 26:563–571. https://doi.org/10.1007/s10904-016-0341-7
18. Karthick R, Sakthivel P, Selvaraju C, Paulraj MS (2021) J Nanomater 2021:8352204. https://doi.org/10.1155/2021/8352204
19. Muniyandi I, Mani GK, Shankar P, Balaguru Rayappan JB (2013) Ceram Int 39:3901–3907. https://doi.org/10.1016/j.ceramint.2013.12.150
20. Ramesh J, Pasupathi G, Mariappan R, Senthil Kumar V, Ponnuswamy V (2013) Optik 124:2023–2027. https://doi.org/10.1016/j.ijleo.2012.06.035
21. Jaramillo TF, Baeck S, Shwarsctein AK, Choi KS, Stucky GD, McFarland EW (2005) J Comb Chem 7:264–271. https://doi.org/10.1021/cc049864x
22. Singh S, Rama N, Ramachandra Rao MS (2006) Appl Phys Lett 88:222111. https://doi.org/10.1063/1.2208563
23. Kim KJ, Park YR (2002) Appl Phys Lett 81:1420–1422. https://doi.org/10.1063/1.1501765
24. Sakthivel P, Muthukumaran S (2017) J Mater Sci Mater Electron 28:8309–8315. https://doi.org/10.1007/s10854-017-6545-y
25. Gayen RN, Rajaram A, Bhar R, Pal AK (2010) Thin Solid Films 518:1627–1636. https://doi.org/10.1016/j.tsf.2009.11.067
26. Abdel-wahab MS, Jilani A, Yahia IS, Al-Ghamdi AA (2016) Superlattices Microstruct 94:108–118. https://doi.org/10.1016/j.spmi.2016.03.043
27. Elilarassi R, Chandrasekaran G (2010) J Mater Sci Mater Electron 22:751–756. https://doi.org/10.1007/s10854-010-0206-8
28. Patil SK, Shinde SS, Rajpure KY (2013) Ceram Int 39:3901–3907. https://doi.org/10.1016/j.ceramint.2012.10.234
29. Samanta A, Goswami MN, Mahapatra PK (2018) J Alloys Compd 730:399. https://doi.org/10.1016/j.jallcom.2017.09.334
30. Srinet G, Kumar R, Sajal V (2013) J Appl Phys 114:033912. https://doi.org/10.1063/1.4813868
31. Iqbal J, Wang B, Liu X, Yu D, He B, Yu R (2009) New J Phys 11:063009. https://doi.org/10.1088/1367-2630/11/6/063009
32. Pal B, Sarkar D, Giri PK (2015) Appl Surf Sci 365:804. https://doi.org/10.1016/j.apsusc.2015.08.163
33. Jadhav J, Biswas S (2016) J Alloys Comp 664:71–82. https://doi.org/10.1016/j.jallcom.2015.12.191
34. Iskendroglua D, Guney H (2017) Ceram Int 43:16593–16599. https://doi.org/10.1016/j.ceramint.2017.09.047
35. Shinde KP, Pawar RC, Shinha BB, Kim HS, Oh SS, Chung KC (2014) Ceram Int 40:16799. https://doi.org/10.1016/j.ceramint.2014.07.148
36. Chithira PR, John TT (2018) J Alloy Compd 766:572–583. https://doi.org/10.1016/j.jallcom.2018.06.336
37. Zeng H, Duan G, Li Y, Yang S, Xu X, Cai W (2010) Adv Func Mater 20:561–572. https://doi.org/10.1002/adfm.200901884
38. Penfold TJ, Szlachetko J, Santomaura FG, Britz A, Gawelda W, Doumy G, March AM, Southworth SH, Rittmann J, Abela R, Chergui M, Christopher JM (2018) Nat Commun 9:478. https://doi.org/10.1038/s41467-018-02870-4
39. Shan FK, Liu GX, Lee WJ, Lee GH, Kim IS, Shin BC (2005) Appl Phys Lett 86:221910. https://doi.org/10.1063/1.1939078
40. Zhao S, Zhou Y, Zhao K, Liu Z, Han P, Wang S, Xiang W, Chen Z, Lü H, Cheng B, Yang G (2006) Phys B 373:154. https://doi.org/10.1016/j.physb.2005.11.116
41. Bylander EG (1978) J Appl Phys 49:1188. https://doi.org/10.1063/1.325059
42. Fabbiyola S, Sailaja V, John Kennedy L, Bououdina M, Judith Vijaya J (2017) J Alloy Comp 694:522. https://doi.org/10.1016/j.jallcom.2016.10.022
43. Elilarassi R, Chandrasekaran G (2011) J Mater Sci Mater Electron 22:751. https://doi.org/10.1007/s10854-010-0206-8
44. Vanheusden K, Warren WL, Seager CH, Tallant DR, Voigt JA (1996) J Appl Phys 79:7983. https://doi.org/10.1063/1.362349
45. Karthika K, Ravichandran K (2015) J Mater Sci Technol 31:1111. https://doi.org/10.1016/j.jmst.2015.09.001
46. Nalluswamy S, Nammalvar G (2019) J Magn Magn Mater 485:297–303. https://doi.org/10.1016/j.jmmm.2019.04.089
47. Dar TA, Agrawal A, Choudhary R, Sen P (2015) Thin Solid Films 589:817–821. https://doi.org/10.1016/j.tsf.2015.07.028
48. Yu W, Yang LH, Teng XY, Zhang JC, Zhang ZC, Zhang L, Fu GS (2008) J Appl Phys 103:093901. https://doi.org/10.1063/1.2903524
49. Ghazi ME, Izadifard M, Ghodsi FE, Yuonesi M (2012) J Supercond Nov Magn 25:101–108. https://doi.org/10.1007/s10948-011-1213-6

50. Dietl T, Ohno H, Matsukura F (2001) Phys Rev B 63:195205. https://doi.org/10.1103/PhysRevB.63.195205
51. Coey JM, Venkatesan M, Fitzgerald CB (2005) Nat Mater 4:173. https://doi.org/10.1038/nmat1310